Environmental Earth Sciences (2020) 79:433
https://doi.org/10.1007/s12665-020-09164-3

ORIGINAL ARTICLE

Assessment of nitrate and heavy metal contamination of groundwater using the heavy metal pollution index: case study of Linares, Mexico

Héctor de León-Gómez[1] · Miguel A. Martin del Campo-Delgado[1] · María V. Esteller-Alberich[2] · Fernando Velasco-Tapia[3] · Efraín Alva-Niño[3] · Arquímedes Cruz-López[1]

Received: 9 March 2020 / Accepted: 3 September 2020 / Published online: 19 September 2020

Abstract

Groundwater contamination is a significant problem in Mexico and around the world. It can be influenced by both natural and anthropogenic factors. In Linares, Mexico, we identified several wells used to cover the water demand for different human activities with nearby potential sources of contamination, including urban, agricultural, and livestock activities, electrical and electronic waste disposal, and fuel storage tanks. We then explored groundwater contamination herein as a result of anthropogenic activities as well as the hydrodynamics of the porous and fractured aquifers in the region based on physiochemical analyses of water samples and the heavy metal pollution index (HPI). The fractured aquifer is composed of shales with a thickness of 70–400 m, while the porous aquifer is composed mainly of gravels, sands, silt, and moderately cemented clays with a thickness of 5 m. The groundwater level is on average 20 m deep, and the flow direction is west to east. The identified water facies are mainly Ca–HCO_3 type, originating from the dissolution of diverse carbonated materials in the area. It was also possible to identify the mixing of groundwater and water influenced by various agricultural and livestock activities, including the use of pesticides and fertilizers and the direct deposition of cattle excreta. The average nitrate concentration of the sampled wells was 80 mg/L, higher than the permissible limit set by the WHO and Mexican standards. The calculated HPI value was 470, well above the critical value of 100, mostly due to the presence of Cd, which is likely associated with the storage of electrical and electronic waste and fuel tanks in the area. These results show that the water wells sampled in Linares, Mexico, without further treatment, are unsuitable for human use. It is important to continue to monitor the contamination of groundwater by heavy metals in different areas of Mexico and to identify potential sources of contamination to create mitigation strategies and ensure the safety and sustainability of water resources in the future.

Keywords Fractured aquifer · Contamination · Nitrates · Heavy metals · HPI

Introduction

Groundwater is intensively used because of its relative abundance, low cost, and ease of collection, transport, and use. However, human activities have greatly impacted water resources, resulting in a decrease in both the quantity and quality of surface water and groundwater, especially in areas dedicated to agricultural and livestock activities (Fetter 2001). Groundwater quality is mainly determined by the chemical and mineral composition of aquifer rocks, geochemical processes, residence time, and other factors related to groundwater flow in addition to effluents or wastes from human activities (Purushotham et al. 2017).

Frequently, hydrogeological studies focus on the amount of available water. However, one of the main problems surrounding the use of groundwater, aside from

✉ Héctor de León-Gómez
hector.deleongm@uanl.edu.mx

[1] Facultad de Ingeniería Civil, Universidad Autónoma de Nuevo León (UANL), San Nicolás de Los Garza, Av. Universidad S/N, Ciudad Universitaria, 66455 San Nicolás de los Garza, Nuevo León, México

[2] Instituto Interamericano de Tecnología y Ciencias del Agua (IITCA), Universidad Autónoma del Estado de México, Carretera Toluca, Ixtlahuaca km. 14.5 San Cayetano Morelos, 50120 Toluca, México

[3] Facultad de Ciencias de la Tierra, Universidad Autónoma de Nuevo León (UANL), Carretera a Cerro Prieto km. 8, Ex Hacienda de Guadalupe, 67700 Linares, NL, México

overexploitation, is contamination. Although groundwater is more difficult to contaminate than surface water, it is also more difficult to eliminate groundwater because of its slow rate of renewal. There are two main types of water contamination processes: punctual processes that affect local areas and diffuse processes that disperse contaminants across large areas (Freeze and Cherry 1979).

In recent years, considerable attention has been placed on the human health risk posed by metals, metalloids, and trace elements in the environment (Rasool et al. 2016). Heavy metals originating from anthropogenic sources can be found in all components of the environment (Assubaie 2015). They are used in various industrial processes and agricultural activities and contained in vehicle emissions, domestic waste, and electrical and electronic waste, including that from a variety of electronic and electrical appliances, such as computers and their accessories, mobile phones and chargers, remote-control units, compact discs, headphones, batteries, televisions, air conditioners, refrigerators, etc. Even though some heavy metals are essential for human health, they can have negative effects in excess amounts (U.S. EPA 2018; WHO 2017; Chowdhury et al. 2016).

Previous studies on the heavy metal contamination of groundwater have revealed that the presence of heavy metals is related to the discharge of untreated water from human activities (Assubaie 2015) or technogenic and industrial activities (Galitskaya et al. 2017). The heavy metal pollution index (HPI), proposed in 1996 by Venkata Mohan et al. (1996), is an effective tool for assessing water quality in terms of heavy metal concentrations that continues to be relevant. In one recent study, for example, Abou Zakhem and Hafez (2015) analyzed heavy metals such as Cd, Pb, Cu, and Zn and found a HPI score of 8.58 based on their mean concentrations, far below the critical value of 100. Similarly, Tiwari et al. (2016) found HPI values below the critical pollution index.

In Mexico, several studies have evaluated the heavy metal contamination of groundwater and its possible causes and effects on groundwater quality. Ocampo-Astudillo et al. (2020) and Salcedo Sanchez et al. (2017) highlighted that the groundwater quality of many urban areas of Mexico is altered by the intensive extraction of groundwater and rapid infiltration of contaminants, including high concentrations of sulphates, calcium, and magnesium and detectable concentrations of F^-, Fe, Mn, Ba, Sr, Cu, Zn, B, and Li. In the groundwater of Emilio Portes Gil, a small town in the state of Puebla, high concentrations of heavy metals, mainly Cr and Pb, were detected and determined to likely result from surface water infiltration and the discharge of untreated urban wastewater to the Atoyac River (Pérez-Castresana et al. 2019).

Another significant cause of groundwater contamination is nitrate (NO_3^-) when present in high concentrations. The presence of NO_3^- in groundwater can be related with anthropogenic activities, such as agriculture and livestock ranching, as well as the discharge of industrial and urban wastewater (Goldberg 1989; Zhai et al. 2017; He et al. 2019; Huljek et al. 2019; Jia et al. 2019). Ravindra et al. (2019) assessed the health risks of groundwater contamination in Chandigarh, India. Based on a physical–chemical analysis of groundwater samples, these authors suggested that the inappropriate disposal of municipal solid waste, dumping of industrial waste, and agricultural activities were the main sources of NO_3^- contamination.

In the present study, we calculated the HPI for the Linares, Nuevo Leon area in northeastern Mexico, with a population of 79,853 inhabitants (INEGI 2015). Practically no studies have been carried out on the quality of groundwater in this area despite numerous potential sources of contamination, such as the landfill, municipal garbage dump, septic tanks, sanitary latrines, agriculture, livestock, and industry. The only study on groundwater quality in this region revealed high concentrations of Cl^- (556 mg/L) through a physical–chemical analysis, but heavy metals were not analyzed (Rangel-Rodriguez 1989). It is important to analyze the presence of heavy metals, given their significant threat to groundwater quality, especially considering that no actions have been taken in the region to prevent or mitigate contamination. Therefore, the objective of the present study was to study the contamination of groundwater by heavy metals and NO_3^- in Linares, Mexico, and in this way, contribute to the knowledge of water quality in the area, since the lack of awareness of users, as well as their lack of education and environmental culture, means that little attention is placed on the problem.

Study area

General framework

The study area is located in the state of Nuevo Leon in northeastern Mexico between 24.7691 and 24.8009 N and − 99.5539 and − 99.5144 W, corresponding with the Topographical Map G14C58 (INEGI 1999). It has an area of 9.37 km^2 (Fig. 1). There is evidence of contamination from anthropogenic activities, including from septic tanks, abandoned diesel stations, abandoned industrial electronic transformers, storage batteries, agricultural machinery, paints and solvents from workshops, electric and electronical waste, and agricultural and livestock activities. Several wells supply drinking and irrigation water in the study area, and these were used as sampling points to measure groundwater levels and take water samples to evaluate water quality.

The climate was confirmed with meteorological data from the Camacho station near the study area. It is semi-arid and

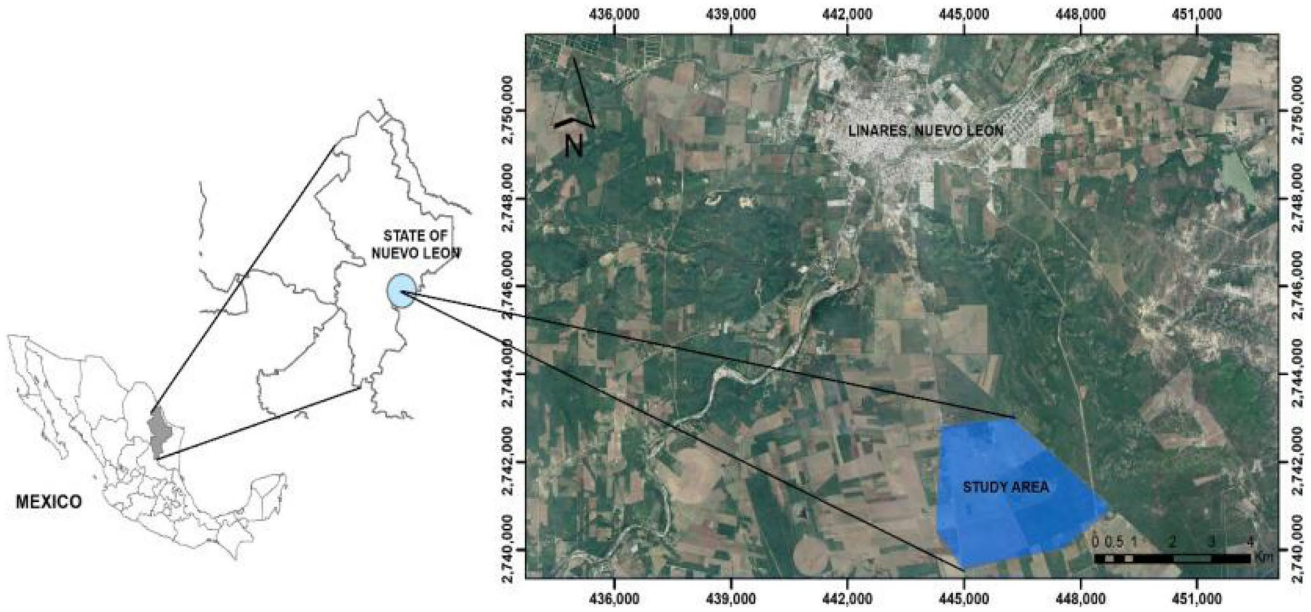

Fig. 1 Map of the study area [elaborated by authors from modified Google Earth image (2020)]

subtropical, with rainfall throughout the year. The annual average temperature is 23.1 °C, with a minimum of 1.5 °C in January and a maximum of 42.5 °C in July. The average annual rainfall is 800 mm, with most rainfall occurring in July and October and the least occurring in June and December. The annual evaporation is 1800 mm. The wind direction is predominantly SE from February to November, but changes to N during January and December.

The study area is located within the San Fernando-Soto La Marina Hydrological Region (RH-25) in the San Fernando River Basin and the Camacho River Sub-Basin. Physiographically, the area forms part of a low topographic plain between two physiographic provinces: the Gulf Coastal Plain (GCP), characterized by relatively moderate folds, and the Sierra Madre Oriental (SMO), characterized by a series of recumbent folds resulting from the transfer of strain from the subduction of the Laramide Orogeny. This folding caused the fracturing of the shale outcrops of the Mendez Formation in the study area, generating calcite-filled faults and small hills (Navarro-Galindo 1959; 1989; López-Ramos 1980).

Geology

The SMO is constituted by sedimentary rocks from the Upper Jurassic to the Upper Cretaceous that are strongly folded and fractured (1982; Fig. 2). It begins in the southern part of the state of Texas in the Big Bend region and extends through Mexico, with a general NNW to SSE direction, ending at the Cofre de Perote, its point of contact with the Mexican Volcanic Belt (MVB). The MVB extends from SW Monterrey in the state Nuevo León to Teziutlán in the state of Puebla and is interrupted on the

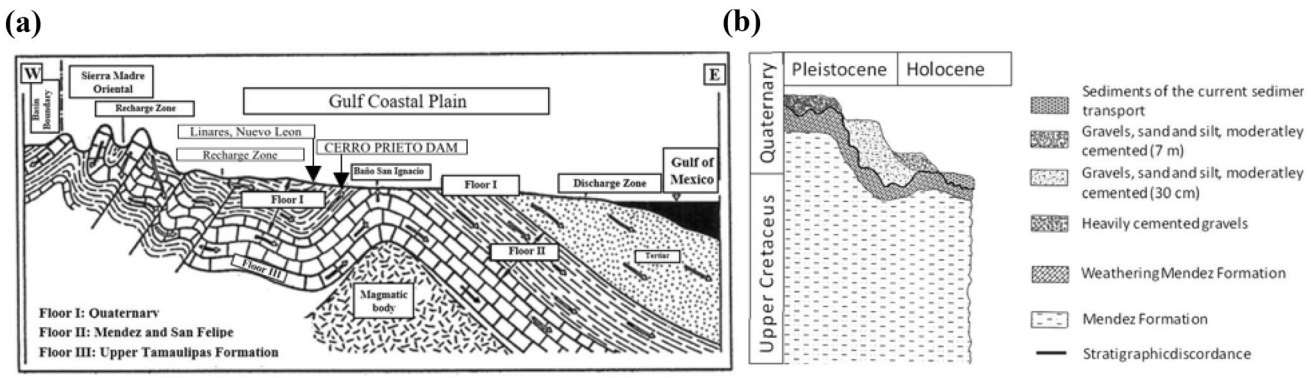

Fig. 2 Cross section (**a**) and stratigraphic column (**b**) of the study area (1982)

surface by igneous spills. In Monterrey, it is flexed, following an E–W path to Torreon in the state of Coahuila; this portion is known as the Monterrey Curvature, with an initial NW–SE course (Navarro-Galindo 1959).

The GCP has an overall flat surface with a mild slope that varies from 200 m in height down to sea level. It is about 2600 km long and 60 to 300 km wide, spanning portions of the states of Tamaulipas, Coahuila, Nuevo León, San Luis Potosí, Veracruz, Puebla, Hidalgo, Oaxaca, Tabasco, Chiapas, Campeche, and Yucatán (Navarro-Galindo 1959).

The San Felipe Formation is 30 km NE of the study area and is mostly formed by a series of compact, thin, and clay-loam limestones. It forms part of the José López Portillo dam curtain, with tight, recumbent folds with vergence to the NE. The thickness of this outcrop is approximately 160 m (1989). It is the upper point of contact between the San Felipe Formation and Mendez Formation. The latter formation is of Campanian Maastrichtian age (Cretaceous) and mainly constituted by shales in addition to marls in the lower portion (Fig. 2a).

Also, it is possible to find deposits of Pliocene age constitute the Cretaceous–Tertiary limit. These deposits are formed by shales, altered marls, gravel lenses, conglomerates, and caliche granules (Fig. 2a). The conglomerate is composed of different fragments, mainly gravels of fluvial origin, flint boulders, and quartzite gravels in a matrix of silt and quartz. The deposits have a general NNE–SSW direction parallel to the SMO with a maximum thickness of 1.5 m (1989).

There are also conglomerate deposits of the Quaternary period with characteristics very similar to the conglomerate unit of the Pliocene except for the degree of compaction (1989; López-Ramos 1980). They are represented by gravel, flint, quartzite, petrified wood, and sediments from rivers and streams. These deposits are found mainly in valleys and foothills and are cemented at the top by a layer of caliche up to 1 m thick. Figure 2b shows the typical geological configuration of the study area.

Hydrogeology

Two types of aquifers were identified: The first is a shallow, porous aquifer that overlies the second, which is constituted by fractured shales and located in a deeper stratum. The porous aquifer is mainly formed by tertiary and quaternary conglomerates with a sand–clay matrix. The average transmissivity is 1.4×10^{-2} m^2/s, and the hydraulic conductivity is 0.035 m/s. Regionally, hydraulic conductivity increases from SW to NE (Galván-Mancilla 1996). Figure 3a shows the heterogeneity of the particles composing this aquifer. Differences are observed in the degree of cementation, with more cementation at the base and little cementation at the surface. The fractured aquifer corresponds with the shales of the Mendez Formation. The fractures are partially filled with calcite. The fracture analysis identified two systems, with the first being oriented NW–SE and the second being oriented NNW–SSE. It has a transmissivity on the order of 8.1×10^{-4} m^2/s, and a hydraulic conductivity of 0.011 m/s (Galván-Mancilla 1996; Rangel-Rodríguez 1989). The average depth of groundwater is 20 m, and the piezometric level is located around 350 m.a.s.l. The flow direction is NW–SE. Figure 3b shows the rocks composing this aquifer, including weathered shales of the Mendez Formation and calcite-filled fractures with a variable thickness of 10–15 cm.

Materials and methods

Piezometric analysis

References on the structure and geological composition of the study area were reviewed to identify the different aquifers and establish the flow and direction of groundwater.

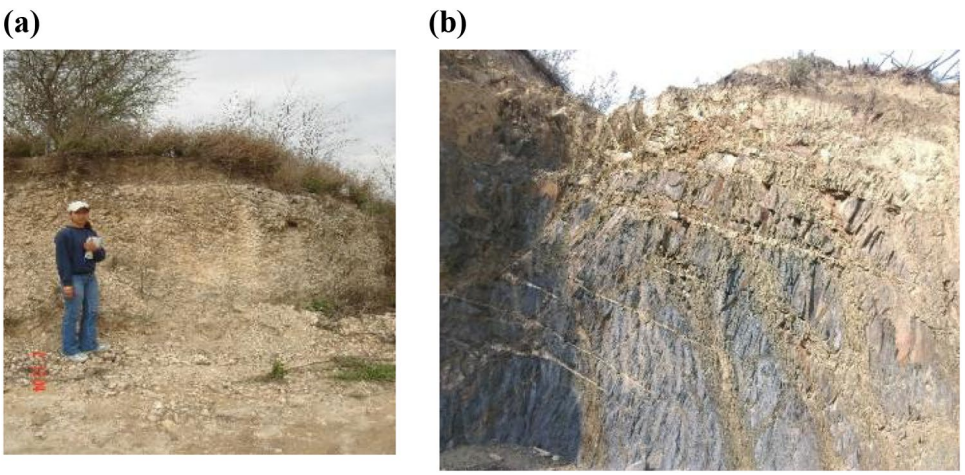

Fig. 3 **a** Porous aquifer material showing cemented conglomerates of 1 cm with intercalations of gravels and imbricate clays 1.5 m thick at their base (24.7983 N, – 99.5385 W). **b** Fractured aquifer material showing a calcite-filled layer 30 cm thick (24.7849 N, – 99.5304 W)

Also, a census of the wells was carried out: 42 wells were identified. However, not all wells were included in the study because they were difficult to access or the required equipment was lacking. Only a total of 26 wells were included, all of which extract water from the fractured aquifer in the Mendez Formation. At each well, the coordinates (UTM), total depth, and groundwater level (Table 1) were recorded using a Magellan 315 GPS, Brunton altimeter, and Solinst 50-m electric probe, respectively. The piezometric levels were determined from the depth of groundwater, and these data were processed in ArcGis 10.3 to calculate the flow direction using the Kriging method and hydrological triangles.

Three sampling campaigns were carried out to measure the depth of groundwater and analyze its behavior during different climate periods of the year. According to the prevailing climate conditions, there are three main seasons: a rainy season, which corresponds with the hurricane season; the ordinary season, which corresponds with a period of regular precipitation; and the dry season, without precipitation. The first sampling was carried out during the ordinary season (March 2018), the second sampling during the rainy season (August 2018), and the final sampling during the dry season (May 2019).

Physical and chemical analysis

Thirteen wells were selected based on their distribution, accessibility, and location near sources of contamination in the study area. These wells are used to extract water for domestic, livestock, and agricultural uses. Samples for physical and chemical analysis were taken in March 2018 (the ordinary season). The physical properties (pH, temperature, and electrical conductivity) were measured in situ with a MultiLine F/SET-3 probe.

Containers of different materials and volumes were first prepared for major ion and heavy metal analysis and, subsequently, for microbiological analysis (Table 2). The water samples for determining major ions (Na^+, K^+, Ca^{2+}, Mg^{2+}, HCO_3^-, Cl^-, SO_4^{2-}, and NO_3^-), minor ions, and heavy metals (Al, Si, Cr, Mn, Fe, Zn, As, Ba, Pb, Hg, Se, Ni, Cd, Sr, Li, Cs, Co, Cu, and Ti) were collected according to the official Mexican norms, and the analyses were carried out at Actlabs Laboratory (Ontario, Canada) using mass spectrometry with induction-coupled plasma (ICP-MS, Thermo X series II model). An electroneutrality balance was applied to these data considering the ranges established by Freeze and Cherry (1979), which was useful for validating the results of the analysis.

The physicochemical data enabled the potential sources of contamination to be identified in neighboring areas with anthropogenic activities or waste disposal (e.g., septic tanks, abandoned diesel stations, abandoned industrial electronic transformers, storage batteries, agricultural machinery, paints and solvents from workshops, electric and electronical waste, and agricultural and livestock activities).

Microbiological analysis

Water samples were collected to determine aerobic mesophilic bacteria and total coliforms at the Laboratory of Clinical and Industrial Analysis of Linares according to the official Mexican norms (Table 2) using the membrane filter (MF) technique (Sartorius, three-branch manifolds). The results were compared with the maximum permissible limits (MPLs) set by the official Mexican norms for human use and consumption (NOM-127-SSA1 1994) and international standards (U.S. EPA 2018; WHO 2017; EEC 2015).

Heavy metal pollution index (HPI)

The heavy metal pollution index (HPI) contemplates the combined influence of the different heavy metals on overall water quality (Sheykhi and Moore 2012), and is based on weighted arithmetic quality mean method. This method considers the establishing of a rating scale giving weightage to selected quality characteristic, as well as selection of pollution parameters on which index is to be based. Rating scale is an arbitrary value (0–1) that can be assessed by making values inversely proportional to the recommended standard for the correspond parameter.

The heavy metal concentration limits were based on Mexican drinking water standards (NOM-127-SSA 1994). The critical HPI value, or the permissible limit for drinking water, is 100 (Venkata Mohan et al. 1996). Samples were analyzed from the same 13 wells analyzed for physicochemical and microbiological parameters.

The HPI model is given as follows (Venkata Mohan et al. 1996):

$$\mathrm{HPI} = \frac{\sum_{i=1}^{n} W_i Q_i}{\sum_{i=1}^{n} W_i}, \tag{1}$$

where w_i is the unit weightage of the ith parameter, Q_i is the sub-index of the ith parameter, and n is the number of parameters considered.

The unit weight (W_i) is determined using the following formula:

$$W_i = \frac{K}{S_i}, \tag{2}$$

where K is the proportionality constant and S_i is the standard permissible limit of the ith parameter.

The sub-index (Q_i) of the parameter is calculated as follows:

Table 1 Data on the location and elevation of wells and the groundwater and piezometric levels during the three sampling seasons (m.*a.s.l.* meters above sea level, *nd* no data)

Id	Name	N latitude	W longitude	Topographic elevation (m.a.s.l.)	Deep well (m)	March 2018 (ordinary season)		August 2018 (rainy season)		May 2019 (dry season)	
						Depth of water table (m)	Piezometric level (m.a.s.l.)	Depth of water table (m)	Piezometric level (m.a.s.l.)	Depth of water table (m)	Piezometric level (m.a.s.l.)
1	P1	24.7958	−99.5327	377	90	24.14	352.86	17.46	359.54	28.31	348.69
2	P4	24.7974	−99.5330	377	75	27.82	349.18	20.21	356.79	31.87	345.13
3	P5	24.7859	−99.5197	360	nd	12.80	347.20	10.73	349.27	12.14	347.86
4	P6	24.7849	−99.5188	358	nd	11.54	346.46	9.47	348.53	10.92	347.08
5	P7	24.7785	−99.5340	368	60	16.36	351.64	12.33	355.67	16.35	351.65
6	P8	24.7776	−99.5334	368	nd	17.16	350.84	13.15	354.85	15.65	352.35
7	P9	24.7835	−99.5378	374	70	19.1	354.9	16.29	357.71	18.39	355.61
8	P10	24.7932	−99.5407	375	75	18.27	356.73	11.5	363.5	17.41	357.59
9	P11	24.7933	−99.5425	376	60	18.83	357.17	13.45	362.55	Dry	Dry
10	P13	24.7941	−99.5421	375	90	18.2	356.8	12.43	362.57	18.35	356.65
11	P14	24.7963	−99.5371	385	110	nd	nd	nd	nd	nd	nd
12	P15	24.7983	−99.5329	380	90	29.96	350.04	23.32	356.68	33.53	346.47
13	P16	24.7970	−99.5377	397	80	42.94	354.06	39.71	357.29	42.9	354.1
14	P17	24.7964	−99.5419	373	nd	nd	nd	nd	nd	nd	nd
15	P19	24.7980	−99.5480	378	60	19.59	358.41	16.56	361.44	19.73	358.27
16	P20	24.7930	−99.5352	375	nd	24.1	350.9	16.38	358.62	23.32	351.68
17	P22	24.7913	−99.5334	370	75	20.27	349.73	12.55	357.45	19.52	350.48
18	P23	24.7927	−99.5311	372	60	21.4	350.6	14.51	357.49	21.63	350.37
19	P24	24.7902	−99.5305	374	110	21.44	352.56	14.55	359.45	21.91	352.09
20	P26	24.7907	−99.5299	371	60	22.11	348.89	15.29	355.71	22.32	348.68
21	P27	24.7897	−99.5299	370	nd	19.33	350.67	11.95	358.05	19.31	350.69
22	P28	24.7836	−99.5294	365	75	nd	nd	nd	nd	nd	nd
23	P31	24.7938	−99.5488	381	nd	23.9	357.1	22.42	358.58	23.42	357.58
24	P33	24.7862	−99.5456	379	60	18.76	360.34	17.8	361.2	18.38	360.62
25	P34	24.7724	−99.5452	380	55	21.57	358.43	19.3	360.7	20.61	359.39
26	P35	24.7789	−99.5490	378	100	19.2	358.8	16.62	361.38	18.1	359.9
27	P36	24.7731	−99.5442	377	nd	21.78	355.22	19.36	357.64	20.7	356.3
28	P38	24.7835	−99.5259	359	nd	12	346	6.1	352.9	11.09	347.91
29	P39	24.7797	−99.5129	356	nd	13.95	342.05	12.35	343.65	13.21	342.79

Table 2 Containers used for the analysis of major ions, heavy metals, and microbiological contents

Analysis	Containers (material and volume)	Preservation
Major and minor ions	Plastic, 1.5 L	4 °C
Heavy metals	HDPE, 60 mL	Filtration, pH < 2, 4 °C
Microbiological	Glass, 100 mL	4 °C

$$Q_i = \sum_{i=1}^{n} \frac{|M_i - I_i|}{S_i - I_i} \times 100, \quad (3)$$

where M_i is the measured heavy metal value of the ith parameter, I_i is the ideal value of the ith parameter, and S_i is the standard value of the ith parameter. A negative sign (−) indicates numerical difference of the two values. However, the ideal value (I_i) is not specified by Mexican drinking water standards, so this variable was not considered in the equation.

Results and discussion

Piezometric study

In March 2018 (ordinary season), the minimum and maximum piezometric levels were 342.05 and 360.34 m.a.s.l., respectively. The average depth of the groundwater table was 20.63 m. Overall, the direction of groundwater flow was W–E and, locally, was SW–NE–E (Fig. 4a). The equal distance between isolines indicates that the permeability of the fractured aquifer is high, which coincides with the pervasive fracturing of the shales of the Mendez Formation.

In August 2018 (rainy season), the groundwater levels varied between 6 and 40 m, with minimum and maximum piezometric values of 343.65 and 363.5 m.a.s.l., respectively. The direction of groundwater flow was NW–SE (Fig. 4b), without significant variation in comparison to the previous season.

In May 2019 (dry season), the maximum piezometric level was 360.62 m.a.s.l., and the minimum was 342.79 m.a.s.l. The average static groundwater level was 20.76 m. The piezometric isolines indicate that the direction of groundwater flow was W–E–SE (Fig. 4c). The flow lines are concentrically oriented toward P39, evidencing the extraction of water and consequent effects on the height of the groundwater table. Notably, one of the wells (P11) was dry due to drought.

The most obvious pattern in groundwater flow between seasons was the marked convergence of the groundwater flow lines in a SE direction, indicating a gradual depletion in the piezometric level. Wells P1 and P4 presented the greatest decrease in the piezometric level. This also occurred in P13, P19, P23, and P26, along with a moderate decrease in the water table. Meanwhile, wells P8, P35, P36, and P38 presented an increase in the piezometric level. The behavior of the groundwater table in the study area suggests that it is affected by the exploitation regimes of specific wells and that is also strongly influenced by climate conditions.

Hydrochemistry

The potential sources of groundwater and surface water contamination in the study area were identified (Table 3). Groundwater quality is also likely affected by geological conditions such as the presence of a highly fractured and weathered rock massif in the fractured aquifer and permeable alluvial sediments in the porous aquifer, increasing the aquifer's vulnerability to pollution.

The physicochemical and microbiological parameters and heavy metal concentrations of the groundwater samples are shown in Tables 4 and 5. The concentrations of Ca^{2+}, HCO_3^-, SO_4^{2-}, and Cl^- are directly related with the water type. Specifically, the Ca^{2+} concentrations were found in the range of 86–620 mg /L, the HCO_3^- concentrations in the range of 270–500 mg/L, the SO_4^{2} concentrations in the range of 27–665 mg/L, the Cl^- concentrations in the range of 43–1500 mg/L, the Na^+ concentrations in the range of 32–770 mg/L, the K^+ concentrations in the range of 3–8 mg/L, the Mg^{2+} concentrations in the range of 9–81 mg/L, and the NO_3^- concentrations were in the range of 20–208 mg/L. The calculated electroneutrality balance (1.6–9%) was within the range recommended by Freeze and Cherry (1979). The implications of these values are discussed at following.

Several water facies were identified in the Piper trilinear diagram (Fig. 5), including Ca–HCO_3, mixed-HCO_3, mixed-mixed, Ca–Cl, and Na–Cl. Three facies were confirmed in the Langelier–Ludwig diagram (Fig. 6), with Ca–HCO_3 being the most abundant group (G1: P6, P13, P14, P16, P17, P22, P28, and P38). Carbon dioxide is the primary source of bicarbonate in the atmosphere, whereas gases dissolved in rain and surface water are the primary source in soil. However, these sources would not necessarily result in high concentrations of bicarbonate in groundwater. In the present scenario, it is likely that the high concentrations of bicarbonate in groundwater are from dissolution of the carbonate materials of the Mendez Formation (Freeze and Cherry 1979). A second group of mixed water was identified (G2: P1 and P24): It was possibly influenced by the dissolution of geological material and various anthropogenic activities. Finally, a third chlorinated water group (G3: P8, P9, and P36) was identified: it was composed of samples with the highest NO_3^- concentrations (128.4–208.1 mg/L), possibly

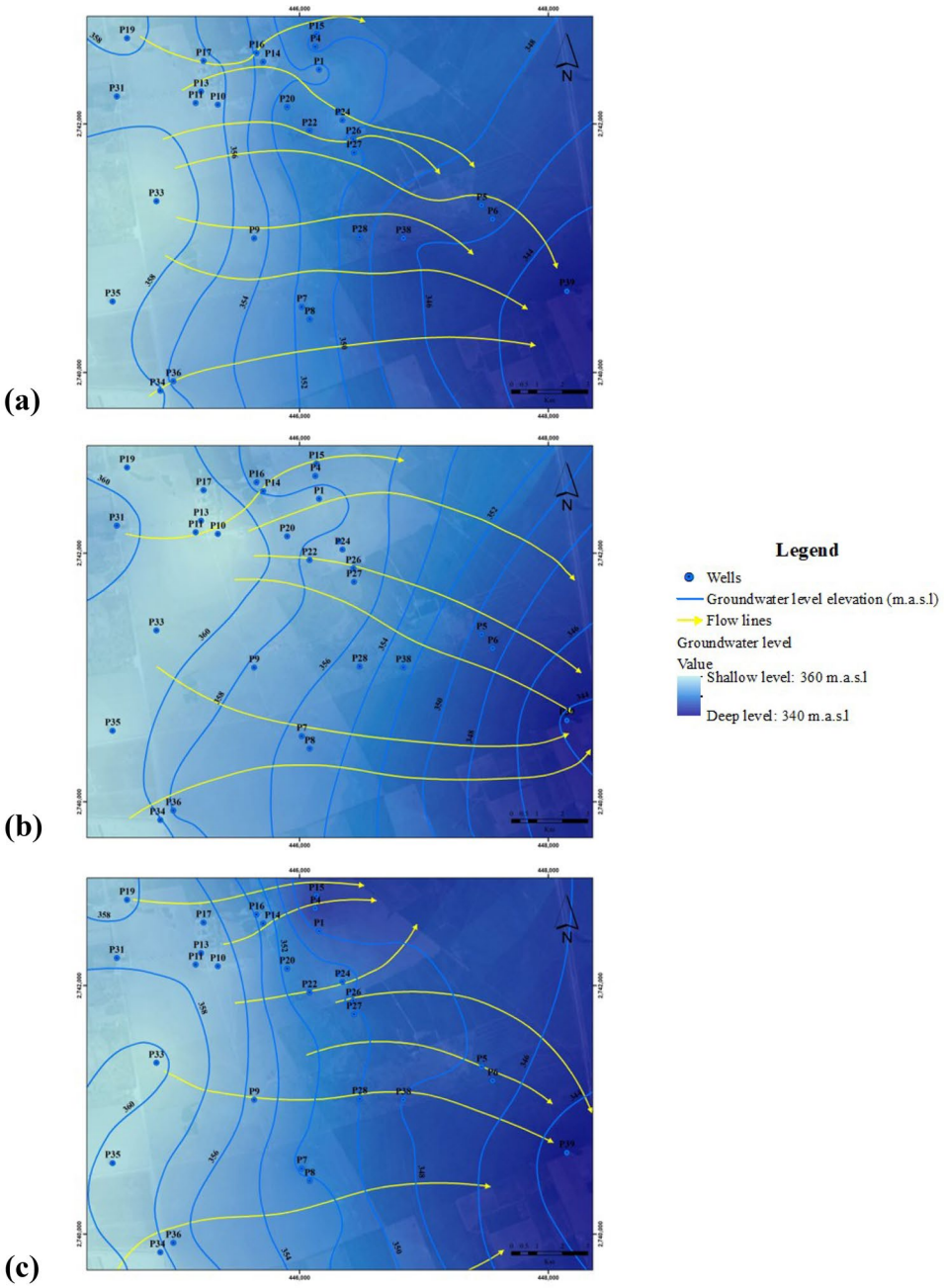

Fig. 4 Groundwater contour map (meters above sea level) for **a** March 2018, **b** August 2018, and **c** May 2019

Table 3 Potential sources of surface water and groundwater contamination

Source of contamination	Contaminants	References
Agricultural and livestock activities, pesticides and fertilizers, and excreta from cattle	TDS, nitrates, fecal coliforms, Cd	Ling (2000); Ramakrishnaiah et al. (2009); Smoroń (2016); Mititelu-Ionus et al. (2019)
Accumulation of electric and electronical waste from computers and their accessories (monitors, printers, keyboards, and central processing units), mobile phones and chargers, remote-control units, etc	Li, Cd, Ba, Sr, Pb, Hg, As, Se, Cr	Wilburn (2008); Awasthi and Li (2017)
Fuel storage tanks, paints, and solvents from workshops	Ba	Nordberg et al. (2001); Otero et al. (2017)

Table 4 Physicochemical and microbiological parameters of groundwater samples in comparison to the standard permissible limits set by drinking water regulations (Data mg/L)

Sample	P1	P6	P8	P9	P13	P14	P16	P17	P22	P24	P28	P36	P38	Drinking water			
														NOM-127-SSA1-1994	U.S. EPA-2018	WHO-2017	EEC-2015
Temperature (°C)	24.0	29.0	26.0	25.0	22.6	25.0	24.0	26.0	25.0	26.0	25.5	26.0	26.0	*	*	*	*
EC (µS/cm)	**1504**	1012	**4890**	**5730**	947	1097	1174	1009	1319	**1503**	737	**5380**	894	*	*	1500	*
pH	6.82	6.56	6.56	6.80	6.62	6.81	**6.49**	6.84	6.61	6.77	6.72	7.19	6.54	6.5–8.5	*	6.5–8.5	6.5–9.5
TDS	**1050**	614	**3481**	**3814**	632	636	713	592	849	944	441	**3618**	523	1000	*	1000	*
TSS	14	17	**524**	**341**	15.0	Nd	6	18	80	28	2	**185**	24	*	*	*	*
Total alkalinity (mg/L $CaCO_3$)	**369.3**	**392.5**	221.6	230.4	299.9	**392.5**	**407.9**	**337.4**	**371.5**	**370.4**	**331.9**	247.0	**344.0**	300	*	*	*
Total hardness (mg/L $CaCO_3$)	497.5	341.2	**1849.1**	**1896.8**	329.8	360.3	419.4	304.2	455.6	**537.6**	299.3	**1058**	312.6	500	*	*	*
Partial hardness	352.9	273.8	1552.3	1561.9	291.2	273.8	308.5	217.9	345.2	370.2	246.8	848.5	275.7	*	*	*	*
Ca^{2+}	140.2	148.8	**616.7**	**620.5**	115.7	108.8	122.6	86.6	137.1	147.1	98.1	**337.**1	149.5		*	*	*
Mg^{2+}	35.1	16.4	72.1	81.3	9.4	21.0	26.9	21.0	26.8	40.6	12.7	50.9	9.0		*	0.4	*
Na^{+}	101.9	43.9	**218.7**	**331.8**	45.2	100.2	65.3	93.1	92.2	99.8	45.3	**771.0**	31.9	200	*	200	200
K^{+}	3.2	3.3	6.0	4.3	3.2	6.6	7.9	4.7	4.7	4.8	4.1	4.3	4.3	*	*	*	*
HCO_3^{-}	400.8	478.8	270.4	281.1	365.9	478.8	497.7	411.6	453.3	451.9	404.9	301.3	419.7	800	*	*	*
Cl^{-}	206.3	64.7	**1354.8**	**1496.3**	83.4	85.4	91.5	104.1	118.3	183.0	43.5	**1249**	58.1	250	*	*	250
SO_4^{2-},	123.1	30.9	**257.6**	**331.3**	42.8	86.4	70.4	53.9	120.2	126.8	27.2	**664.3**	37.9	400	*	250	150
NO_3^{-}	**79.0**	**71.0**	**128.4**	**128.4**	**65.9**	20.9	**75.3**	**29.4**	**82.6**	**83.0**	26.0	**208.1**	**44.6**	44.3	44.3	50	50
Total coliforms (MPN/100 mL)	**79**	**64**	**78**	**96**	**85**	**96**	**75**	**165**	**130**	**25**	**86**	**126**	**142**	0	*	0	0
Aerobic mesophilic bacteria	1060	850	885	859	1240	1205	850	1369	1089	416	956	1240	1096				

Values in bold exceed the permissible limits

TDS total dissolved solids, *TSS* total suspended solids

Table 5 Minor ion and heavy metal concentrations of groundwater samples in comparison to the standard permissible limits set by drinking water regulations (Data mg/L)

Sample	P1	P6	P8	P9	P13	P14	P16	P17	P22	P24	P28	P36	P38	Drinking water			
														NOM-127-SSA1-1994	U.S. EPA-2018	WHO-2017	EEC-2015
Al	<0.002	<0.002	<0.002	<0.002	<0.002	<0.002	<0.002	<0.002	<0.002	<0.002	<0.002	<0.002	<0.002	0.20	*	0.2	0.2
Si	14.7	16.0	<0.2	<0.2	14.10	14.90	20.10	15.70	15.70	16.30	14.30	<0.2	14.60		*	*	*
Cr	<0.0005	<0.0005	<0.0005	<0.0005	0.0034	0.002	0.0009	0.0006	<0.0005	<0.0005	0.0016	<0.0005	0.0021	0.05	0.01	0.05	0.05
Mn	0.0016	<0.0001	0.010	<0.0001	0.0002	0.0124	0.0024	<0.0001	0.0008	0.0005	0.0016	<0.0001	<0.0001	0.015	0.05	0.4	0.05
Fe	<0.01	<0.01	<0.01	<0.01	<0.01	<0.01	<0.01	<0.01	<0.01	<0.01	<0.01	<0.01	<0.01	0.30	0.3	0.3	0.2
Zn	0.0122	0.0014	<0.0005	0.05	0.0032	0.0387	0.0956	0.0042	0.0081	0.005	0.0093	<0.0005	0.0015	5.0	5.0	*	*
As	0.00019	0.00018	<0.00003	<0.00003	0.00041	0.00029	0.00026	0.00017	0.00039	0.00022	0.00018	<0.00003	0.00039	0.025	0.01	0.01	0.01
Ba	0.0586	0.0994	**0.33**	**0.40**	0.137	0.0976	0.074	0.121	0.0794	0.099	0.0707	0.100	0.114	0.70	2.0	0.5	*
Pb	<0.00001	<0.00001	<0.00001	<0.00001	<0.00001	<0.00001	0.00004	0.00002	0.00003	0.00013	0.00006	<0.00001	<0.00001	0.025	0.015	0.01	0.01
Hg	<0.0002	<0.0002	<0.0002	<0.0002	<0.0002	<0.0002	<0.0002	<0.0002	<0.0002	<0.0002	<0.0002	<0.0002	<0.0002	0.001	0.002	0.006	0.001
Se	0.0058	0.002	<0.0002	<0.0002	0.0026	0.0037	0.002	0.0036	0.003	0.0061	0.0009	<0.0002	0.0025	*	0.05	0.04	0.01
Ni	0.0011	<0.0003	<0.0003	<0.0003	0.0019	0.0011	0.0024	0.0004	0.0007	0.0005	0.0006	<0.0003	0.0011	*	*	0.07	*
Cd	**0.03**	<0.00001	<0.00001	<0.00001	**0.04**	**0.01**	**0.06**	<0.00001	**0.01**	<0.00001	**0.03**	<0.00001	<0.00001	0.005	0.005	0.003	0.005
Sr	<0.00004	<0.00004	**9.77**	**12.0**	<0.00004	<0.00004	<0.00004	<0.00004	<0.00004	<0.00004	<0.00004	**7.0**	<0.00004	*	4.0	*	*
Li	0.085	0.058	**0.20**	**0.20**	0.019	0.091	0.047	0.066	0.052	0.070	0.032	**0.40**	0.022	*	0.2	*	*
Cs	0.000376	0.000025	0.0002	<0.0000001	0.000009	0.00114	0.000381	0.000615	0.000389	0.000468	0.000023	0.0007	0.00002	*	0.001	*	*
Co	<0.000005	<0.000005	<0.000005	<0.000005	<0.000005	0.000108	0.000027	<0.000005	0.000013	<0.000005	<0.000005	<0.000005	<0.000005	*	*	*	*
Cu	0.0018	0.0003	<0.0002	<0.0002	<0.0002	<0.0002	0.0017	<0.0002	0.0005	0.0014	0.0014	<0.0002	<0.0002	2.0	1.0	2.0	2.0
Ti	0.0017	0.0018	<0.000001	<0.000001	0.0017	0.0018	0.0025	0.0017	0.0018	0.0019	0.0017	<0.000001	0.0014	*	*	*	*

Values in bold exceed the permissible limits

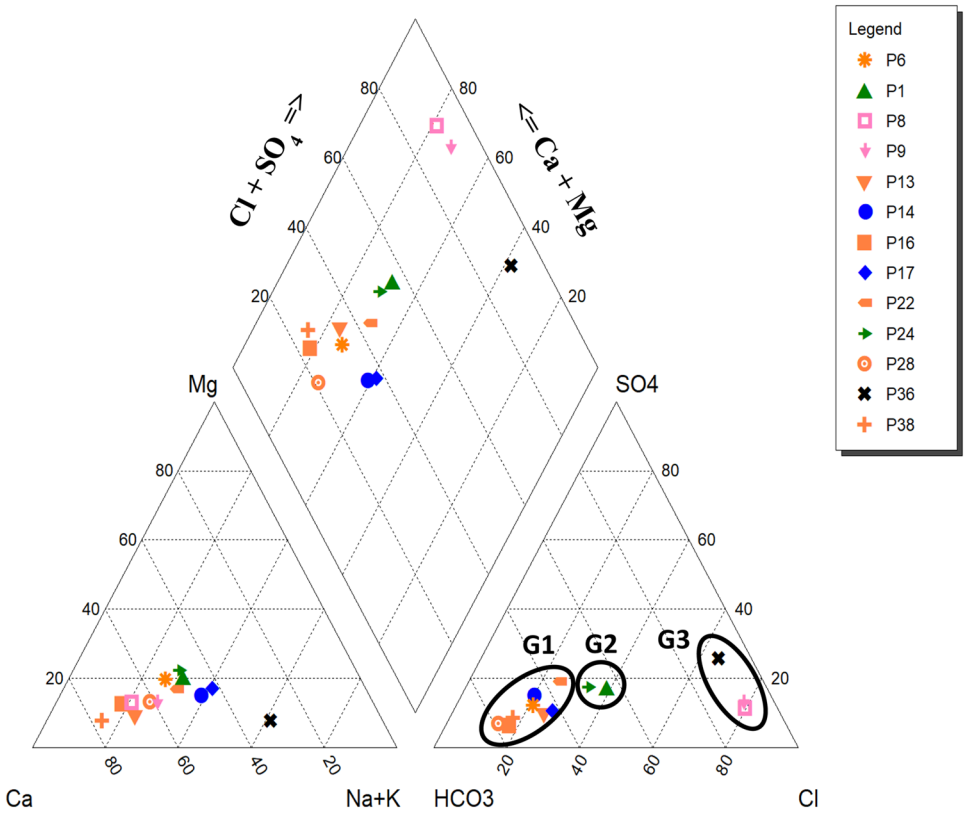

Fig. 5 Piper trilinear diagram of groundwater samples

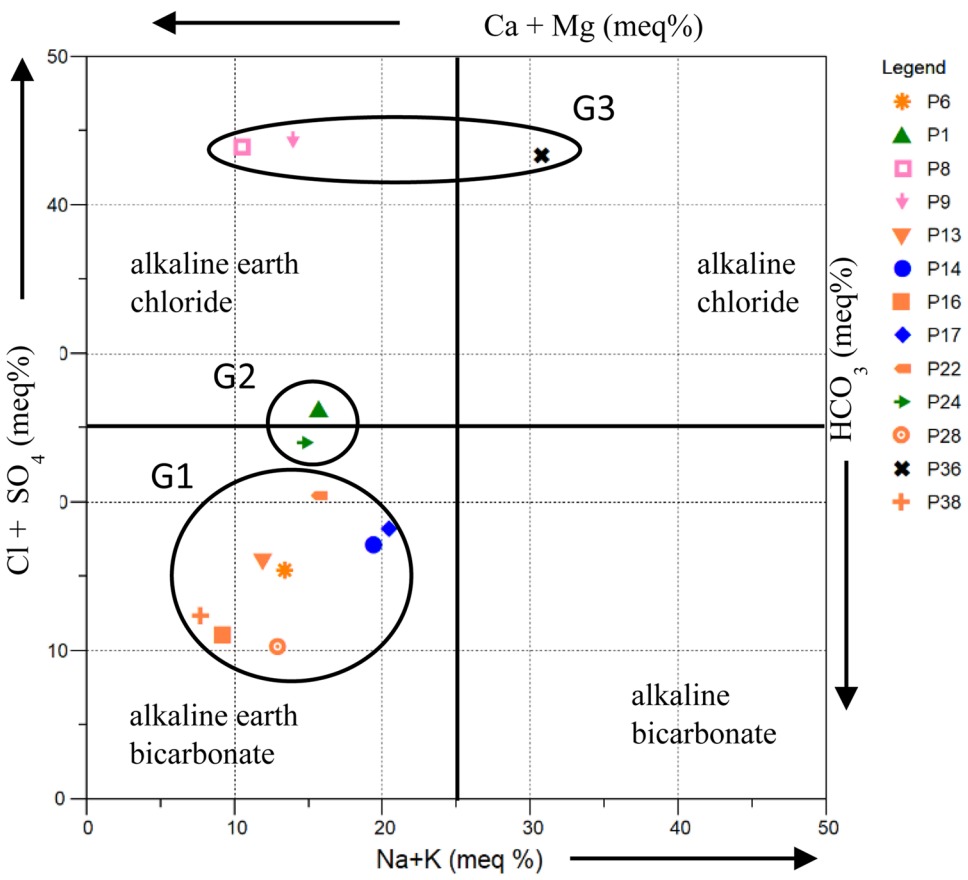

Fig. 6 Langelier–Ludwig diagram of groundwater samples

reflecting the impact of agricultural and livestock activities. The Stiff diagram at each sampling point shows the spatial distribution of the three water facies, NW–SE, (Fig. 7) as occurs with water flow.

The relationships among physicochemical parameters were statistically explored with a correlation coefficient matrix (Table 6). If the correlation coefficient r is > 0.7, the two parameters are considered strongly correlated, whereas if the value r is between 0.5 and 0.7, a moderate correlation is indicated (Koh et al. 2009). The matrix showed that the EC increased as the most abundant ions increased ($r > 0.7$). This is logical given that this chemical

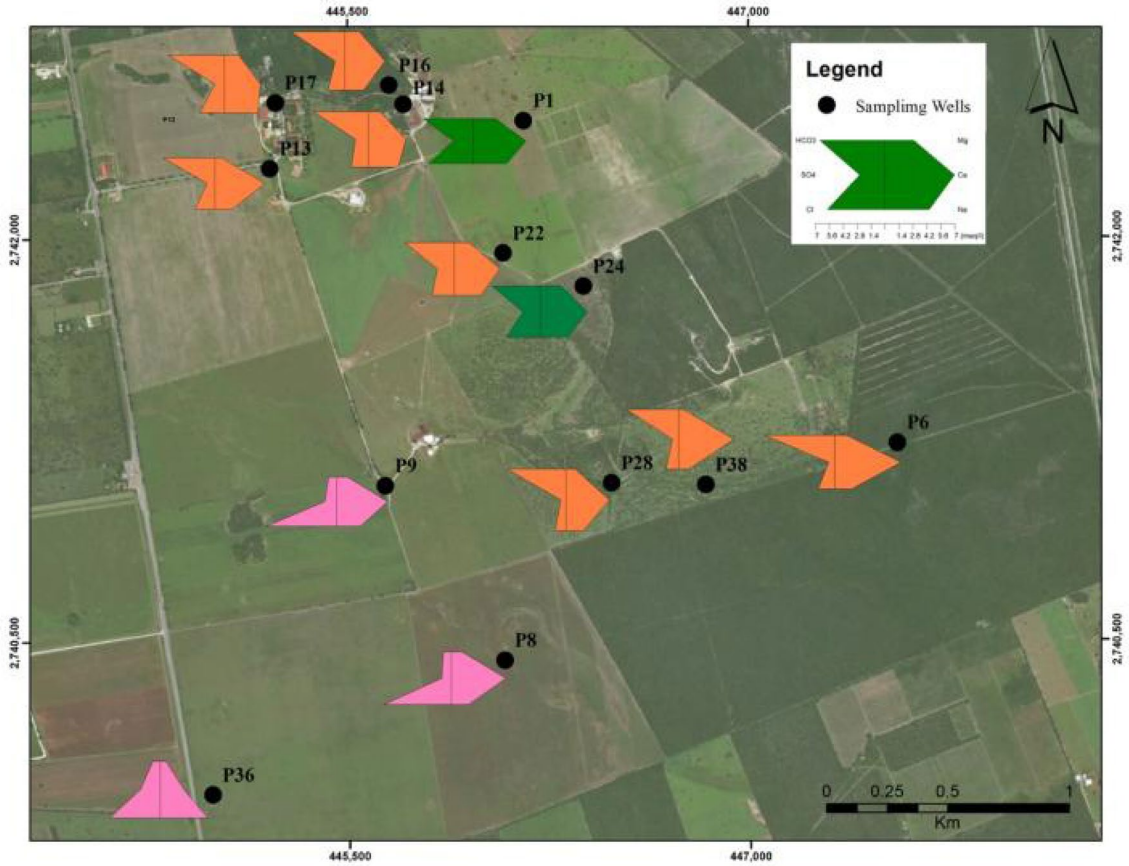

Fig. 7 Stiff diagrams of selected wells in the study area (G1: orange, G2: green, G3: pink)

Table 6 Correlation coefficients among the physicochemical characteristics of groundwater samples

	HCO_3^-	SO_4^{2-}	Cl^-	NO_3^-	Na^+	K^+	Ca^{2+}	Mg^{2+}	T.C	pH	E.C
HCO_3^-	1.00	−0.70	−0.82	−0.62	−0.69	0.47	−0.75	−0.62	−0.26	−0.26	−0.74
SO_4^{2-}		1.00	**0.87**	**0.88**	**0.99**	−0.05	**0.67**	0.70	0.17	0.60	**0.79**
Cl^-			1.00	**0.76**	**0.84**	−0.09	**0.95**	**0.88**	0.12	0.30	**0.86**
NO_3^-				1.00	**0.84**	−0.22	0.61	0.69	−0.05	0.47	**0.86**
Na^+					1.00	−0.04	0.63	0.63	0.22	0.66	**0.75**
K^+						1.00	−0.1	−0.01	0.02	−0.16	−0.21
Ca^{2+}							1.00	**0.88**	0.04	0.04	**0.80**
Mg^{2+}								1.00	−0.12	0.13	**0.83**
T.C									1.00	0.25	**0.97**
pH										1.00	**0.88**
E.C											1.00

Values in bold have correlation coefficients > 0.7

TC total coliforms, *EC* electrical conductivity

property is determined by the most abundant ions, which in turn determine the water facies identified in the Piper and Langelier–Ludwig diagrams.

The Cl^- content increased as the Na + content increased ($r > 0.8$). Also, Cl^- was correlated with Ca^{2+}, Mg^{2+}, and SO_4^{2-}. Notably, NO_3^- was correlated with SO_4^{2-} and Cl^- ($r > 0.7$), which is consistent with its assumed anthropogenic origin. However, strong correlations were not found between HCO_3^- and the rest of the evaluated variables. It is important to further explore this lack of correlation, because it is not congruent with the geological environment of the aquifer.

The relationships between HCO_3^- and $Ca^{2+} + Mg^{2+}$ are shown in Fig. 8a. It is possible to observe that all points of groups G1 and G2 are located on the line $y = 2x$ (or in its proximity), which corresponds with the dissolution of carbonates (Biswas et al. 2012; Rajmohan et al. 2017; Canora et al. 2019), whereas the samples of the group G3 are distanced from this line as well as the line $y = x$. This same behavior is observed in Fig. 8b for the relationship between HCO_3^- and $Na^+ + K^+$. These data indicate that there is an intense process acting on the G3 samples causing enrichment with cations, such as ion exchange. To verify the ion exchange process, the relationship of $(Ca^{2+} + Mg^{2+}) - (HCO_3^- + SO_4^{2-})$ vs. $(Na^+ - Cl^-)$ was graphed (Fig. 8d). The $Ca^{2+} + Mg^{2+}$ values were corrected with $HCO_3^- + SO_4^{2-}$ to exclude the contribution of ions from carbonates and silicates. The Na^+ concentration was corrected with Cl^- to exclude Na^+ from atmospheric deposition (Biswas et al. 2012; Esteller et al. 2017). In aquifers affected by ion exchange, the adjustment of data to a straight line with a negative slope suggests the existence of an ion exchange process. In the present case, the G1 and G2 groups are located at the intersection of the axes, indicating that no exchange process is occurring (Fig. 8d). On the other hand, the G3 group is affected by an exchange process causing the fixation of Na^+ and release of Ca^{2+} and Mg^{2+} from the rock matrix, with the exception of the P36 sample. This latter sample seems to be affected by the dissolution of salts and chemical products used in agricultural and livestock activities and also is located on the line $y = x$ (indicating halite dissolution), as observed in Fig. 8c.

Nitrate pollution

Nitrate along with Cl^-, SO_4^{2-}, and total coliforms are indicators of pollution from urban, industrial, and agricultural activities, which can contribute amounts significantly above those naturally found in groundwater (Lang et al. 2006; Marshall et al. 2019). Specifically, NO_3^- originates from the

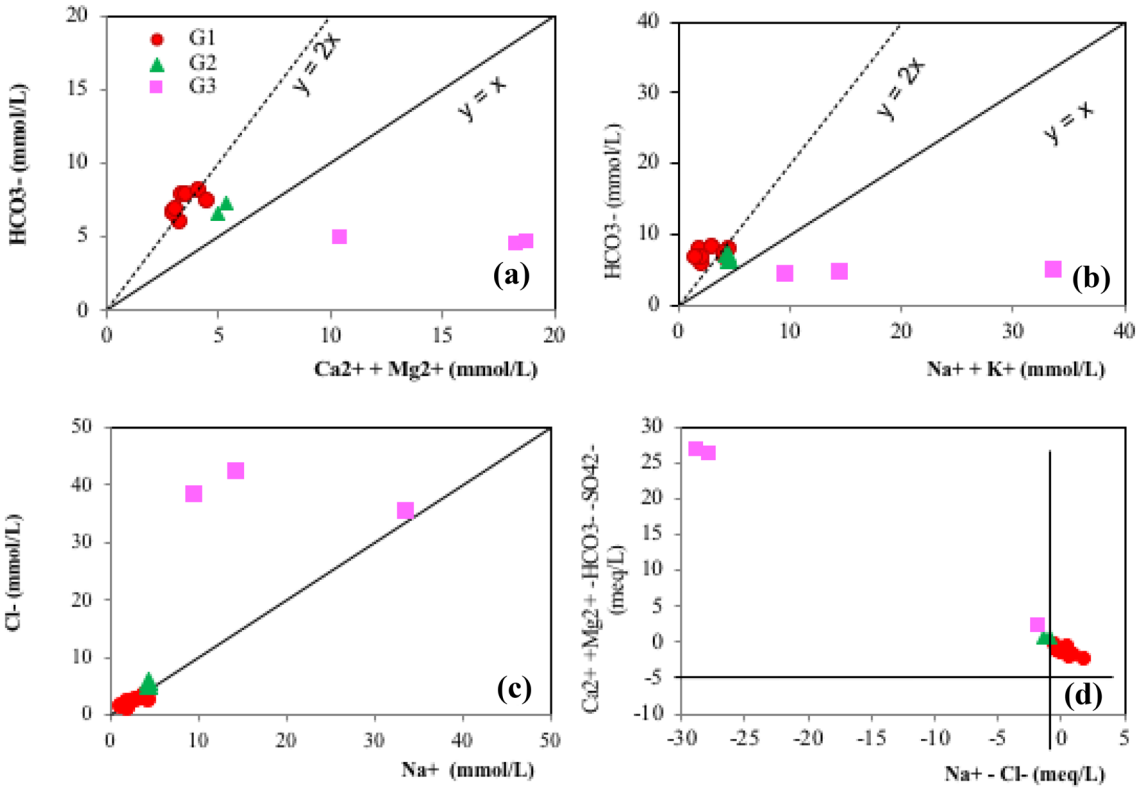

Fig. 8 Scatter plots of selected ions in groundwater samples. **a** HCO_3^- versus $Ca^{2+} + Mg^{2+}$, **b** HCO_3^- versus $Na^+ + K^+$, **c** Cl^- versus Na^+, and **d** $(Ca^{2+} + Mg^{2+}) - (HCO_3^- + SO_4^{2-})$ versus $Na^+ - Cl^-$

excreta and urine of cattle, septic tanks, and use of fertilizers in sorghum forage crops. Also, plowing, fallowing, and irrigation (large sheets of irrigation) directly affect the dissolution of fertilizers and transport them.

The relationships between NO_3^- and the other pollution indicators are shown in Fig. 9 (Pujari et al. 2012; Ximenes et al. 2018). Total coliforms and NO_3^- concentrations are particularly important because they determine whether groundwater is apt for human consumption. In this sense, it is important to consider that septic tanks, dumping of excreta from cattle, and organic matter decomposition can cause nitrates and total coliforms increase (Ling 2000; Ramakrishnaiah et al. 2009; Smoron 2016; Mititelu-Ionus et al. 2019).

Most of the collected samples are contaminated and show similar behavior (G1 and G2). The G3 samples, which are the most affected by pollution from septic tanks and agricultural and livestock activities, have the highest total coliform concentrations with respect to NO_3^-.

Heavy metal pollution index (HPI)

The minor ion and heavy metal concentrations are shown in Table 5. The highest concentrations were found for Sr, Li, Cd, and Ba. Sr is a natural element found in rocks, soils, and oil derivatives, but it could originate from the diesel tanks of service stations for agricultural machinery. Li also is present rocks (igneous rocks), brines, clays, and oil wells. However, its origin in the present scenario could be a dump for agricultural machinery, batteries, grease, and lubricants. In high concentrations, it has negative effects on human health, causing disorders of the thyroid gland and kidney damage (U.S. EPA 2018). Cd can be found in the Earth's crust, always in combination with Zn, and is used in different industrial products and processes (Blanco-Hernandez et al. 1998; Nordberg et al. 2001). In the study area, it likely comes from rusty machinery, including agricultural machinery, and storage batteries, both of which are stored under outdoor conditions. Also, it is possible that Cd is contained in pesticides, excreta, and manure. Finally, the origin of Ba is likely a workshop where paints are used and an electronic waste deposit. Ba can also be found in the environment naturally due to the erosion of rocks and runoff water from croplands. It is also used in different industries and in paints, ceramics, paper, cement, rubber, and rat poison, for example (De Zuane 1993).

The HPI value calculated from the average heavy metal concentrations was 470 (Table 7), well above the maximum limit of 100 established by Venkata Mohan et al. (1996), which has also been used by other authors as a reference

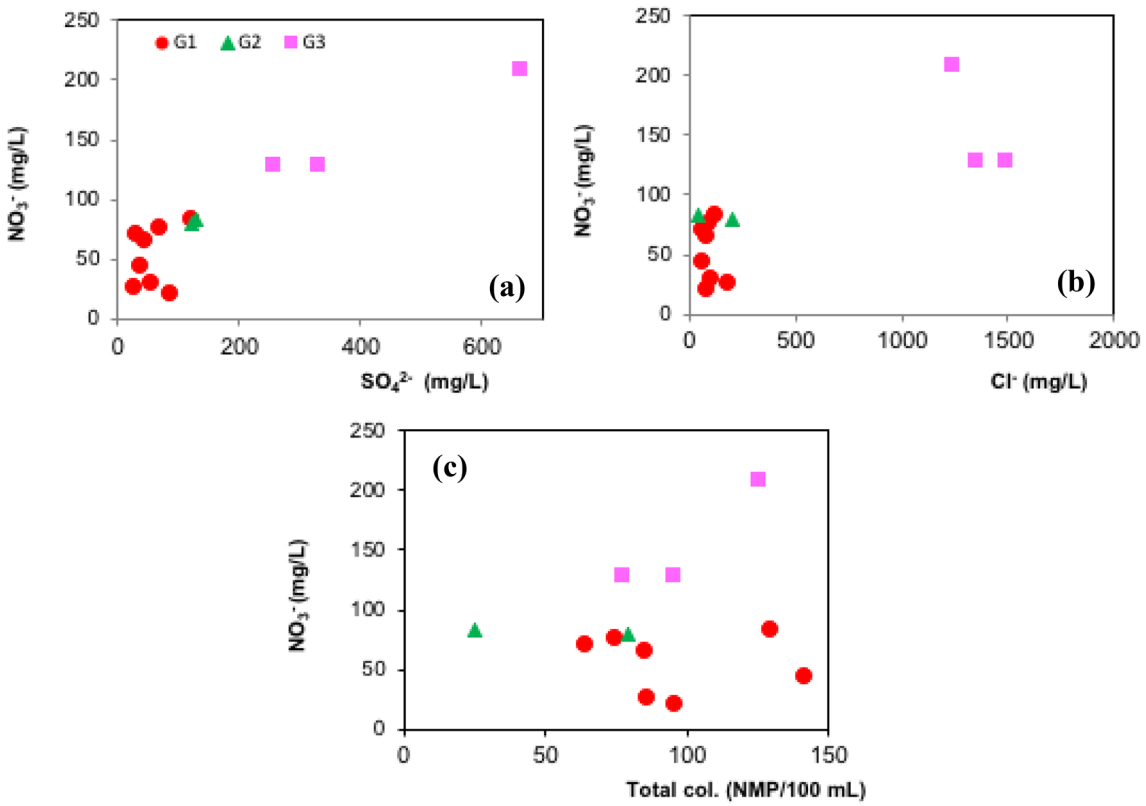

Fig. 9 Scatter plots of **a** NO_3^- vs. SO_4^{2-}, **b** NO_3^- vs. Cl^-, and **c** NO_3^- vs. total coliforms to illustrate NO_3^- contamination of groundwater

Table 7 Heavy metal pollution index (HPI) of the study area

Heavy metals	Mean value (µg/L) (M_i)	Standard permissible limit (µg/L) (S_i)	References	Unit weightage (W_i)	Subindex (Q_i)	$W_i \times Q_i$
Ba	142	700	NOM-127	0.0014	20.337	0.030
Ni	1	20	WHO 2017	0.05	5.05	0.252
Cd	30	5	NOM-127	0.2	600	120
Sr	9590	4000	U.S. EPA-2018	0.00025	239.75	0.060
Li	103	200	U.S. EPA-2018	0.005	51.615	0.258

$\sum W_i = 0.26 \sum W_i Q_i = 120.599 \quad \text{HPI} = \frac{\sum_{i=1}^{n} W_i Q_i}{\sum_{i=1}^{n} W_i} = 469.846$

(Nalawade et al. 2012; Kwaya et al. 2019). This value reflects the high Cd concentrations as well as the pollution load from several elements as a whole.

The HPI values were also calculated for each sampling point to enable a comparison of water quality between the sampling points (Table 8). The values of P1, P13, P14, P16, P22, and P28 exceeded the maximum limit and reflected the highest concentrations of Cd (Table 5). Notably, no G3 sample had a high HPI value.

Water quality

Drinking water

The EC in wells P1, P8, P9, P24, and P36 exceeded the limits established by the WHO (2017; Table 4). Also, the TDS concentrations in wells P1, P8, P9, and P36 exceeded the limits (1000 mg/L) established by the WHO (2017) and NOM-127-SSA1 1994. The highest TSS values appeared in the wells with the highest TDS values (P8, P9, and P36), with the exception of well P1, which had a TSS of 14 mg/L (Table 4).

Similarly, the total alkalinity concentrations in wells P1, P2, P14, P16, P17, P24, P28 and P38 exceeded the limit (300 mg $CaCO_3$/L) established by NOM-127-SSA1 1994, with values ranging from 331.9 to 407.9 mg $CaCO_3$/L. Also, the total hardness concentration in wells P8, P9, P24, and P36 exceeded the limit (500 mg $CaCO_3$/L) considering the same standard (Table 4), with values ranging from 537.6 to 1896.8 mg $CaCO_3$/L.

The high Cl^- concentrations present in wells P1, P8, P9, and P36 were above the limits (250 mg Cl^-/L) established by NOM-127-SSA1 (1994) and EEC (2015) (Table 4). Na^+ concentrations exceeding the limits (200 mg Na^+/L, NOM-127-SSA1 1994, WHO 2017 and EEC 2015) were also found in P8, P9, and P36 (Table 4). SO_4^{2-} concentrations exceeded the limit (400 mg/L) established by NOM-127-SSA1 (1994) in well P36 (664.3 mg/L) and exceeded the limits established by the WHO (2017) and EEC (2015; Table 4) in wells P8 and P9, with values of 257.6 and 331.3 mg/L, respectively.

Notably, the NO_3^- concentrations exceeded the established limits in almost all sampled wells, except P14 and P28 (Table 4). The adverse effects of high concentrations of NO_3^- in drinking water are cyanosis (in children), respiratory difficulties, methemoglobinemia, and spontaneous

Table 8 Heavy metal concentrations (µg/L) and HPI values of groundwater samples (*no data)

	Sampling Station	Ba (µg/L)	Ni (µg/L)	Cd (µg/L)	Sr (µg/L)	Li (µg/L)	HPI
G1	P6	99.4	0.3	*	*	58	0.94
G1	P13	137	1.9	40	*	19	625.49
G1	P14	97.6	1.1	10	*	91	157.87
G1	P16	74	2.4	60	*	47	937.88
G1	P17	121	0.4	*	*	66	1.13
G1	P22	79.4	0.7	10	*	52	157.09
G1	P28	70.7	0.6	30	*	32	468.46
G1	P38	114	1.1	*	*	22	1.38
G2	P1	58.6	1.1	30	*	85	469.46
G2	P24	99	0.5	*	*	70	1.25
G3	P8	400	*	*	9770	200	2.50
G3	P9	400	*	*	12,000	200	2.56
G3	P36	100	*	*	7000	400	4.15

abortions, as well as the corrosion of water pipes (De Zuane 1993; U.S. EPA 2018). Likewise, total coliforms exceeded the limits in all sampled wells (Table 4). According to the established standards, drinking water should not contain coliforms, as the consumption of water with high concentrations of coliforms can cause intestinal diseases such as hepatitis A and E, typhoid, dysentery, diarrhea, and cryptosporidiosis (Ling 2000).

On the other hand, the results of the bacteriological analyses indicated that 50% of the collected samples have < 956 MPN/mL of aerobic mesophilic bacteria, reflecting contamination in addition to the existence of favorable conditions for the multiplication of microorganisms and presence of organic matter. The remaining samples had values exceeding 1000 MPN/mL, with a maximum of 1369 MPN/mL (Table 4). Notably, the highest concentrations of aerobic mesophilic and total coliforms occur in the NW zone of the study area (P13, P14, and P17).

As mentioned, high concentrations of several heavy metals (Sr, Li, Ba, and Cd) were found (Table 5). High concentrations of Sr (7.0–9.77 mg/L) were detected in P8, P9, and P36; these concentrations exceeded the maximum permissible limit (4.0 mg/L) according to the U.S. EPA (2018; Table 4). Exposure to high levels of Sr can alter the growth of children's bones and produce anemia and blood clotting disorders (U.S. EPA 2018).

Li concentrations exceeded the quality limit (0.20 mg/L) in P8, P9, and P36 (0.20–0.40 mg/L) according to the U.S. EPA (2018; Table 5). According to the WHO (2017), these concentrations did not exceed the limit established for Ba; however, in wells P8 and P9, Ba concentrations were close to the established limit (0.30 and 2.0 mg/L, respectively).

Cd concentrations exceeded the quality limit (0.003–0.005 mg/L) in wells P1, P13, P14, P16, P22, and P28 (Table 5). Similar to aerobic mesophilic bacteria and total coliforms, the highest concentrations of Cd were found in the NW part of the study area (Fig. 10).

Irrigation water

In regard to the quality of water for irrigation, four categories were detected: (a) group C2-S1, with medium saline water; (b) group C3-S1, with highly saline water and low sodium concentrations; (c) group C4-S2, with extremely saline water and medium sodium concentrations; and (d) the samples from wells P9 and P36, which were not classified

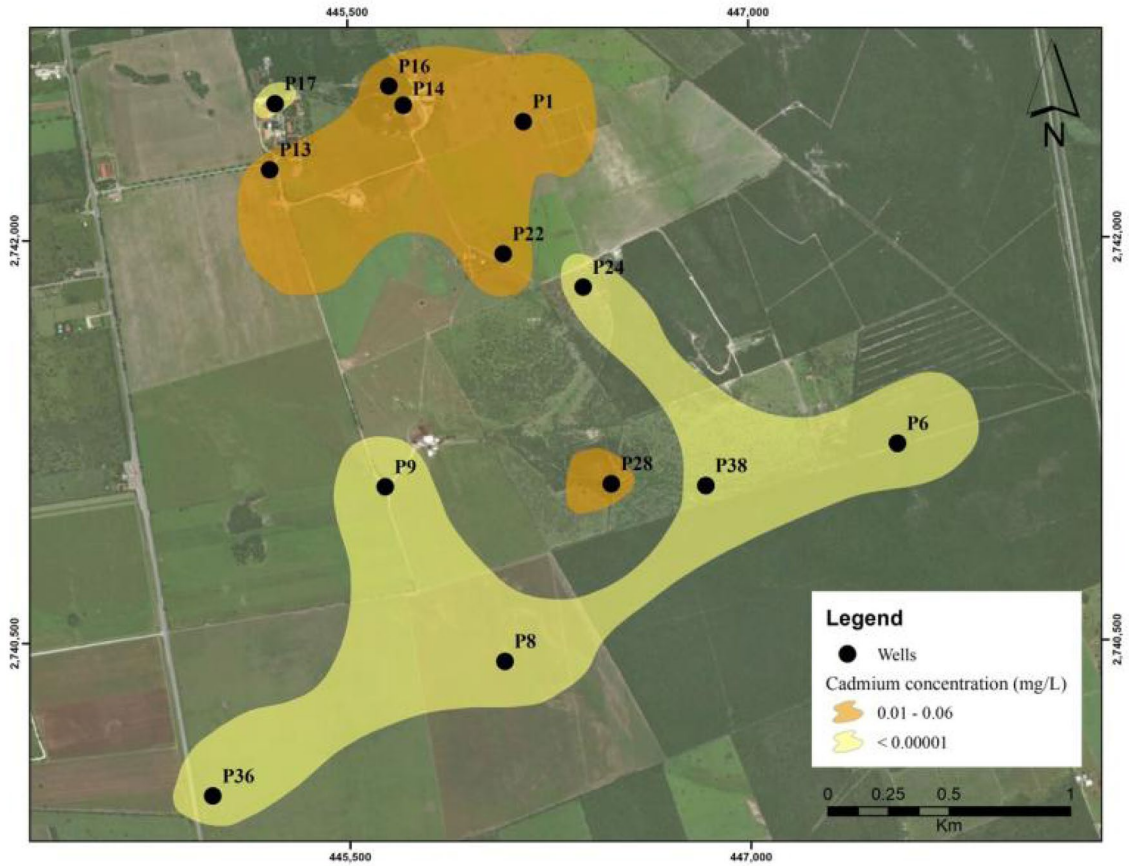

Fig. 10 Distribution of Cd in the study area

because their EC values exceed the maximum values that can be inputted to the Wilcox diagram. However, these latter samples would be considered to have high alkalinity and conductivity (C4-S4; Fig. 11).

Conclusions

The physical characteristics of the study area (climatology, soil type, geology, and water availability) have favored agricultural and livestock activities over the last 40 years. However, these activities have altered the availability and quality of groundwater.

In the study area, it is clear that the geological media influence the infiltration and transport of pollutants, because is composed mainly of gravels, sands. The depth of the groundwater levels ranged from 20.63 to 20.76 m. The configuration of the piezometric isolines indicates high permeability in the fractured aquifer. The general direction of groundwater flow is W–E–SE, coinciding with the fracturing system. There is a hydraulic connection between the fractured aquifer (Mendez Formation) and porous aquifer (Quaternary conglomerates), favoring pollution transport and contributing to the accelerated chemical alteration of groundwater quality.

The evaluation of the physicochemical characteristics of groundwater revealed three water facies. One is related with the dissolution of carbonated material. The other is related with the mixing of water influenced by the dissolution of geological material and agricultural activities. The final reflects the possible impact of fertilizer use, septic tanks, and livestock activities.

With respect to water quality, the NO_3^- and coliform concentrations are the main factors constraining the suitability of groundwater for human consumption in the study area. The high NO_3^- concentrations found at most wells were related with total coliform concentrations, and these are likely derived from septic tanks and agricultural and livestock activities.

The HPI values based on the concentrations of Sr, Li, Ni, Ba, and Cd revealed critical water contamination that can be attributed to the high concentration of Cd (50% of the sampled wells) likely resulting from electrical and electronic waste.

The results obtained, show that the pollution from point sources and human activities identified at study area, represent a risk to the quality, quantity, and conservation of groundwater. For this reason, it is important to continue to assess groundwater contamination in this area and other areas of Mexico, as the provision of clean water is necessary

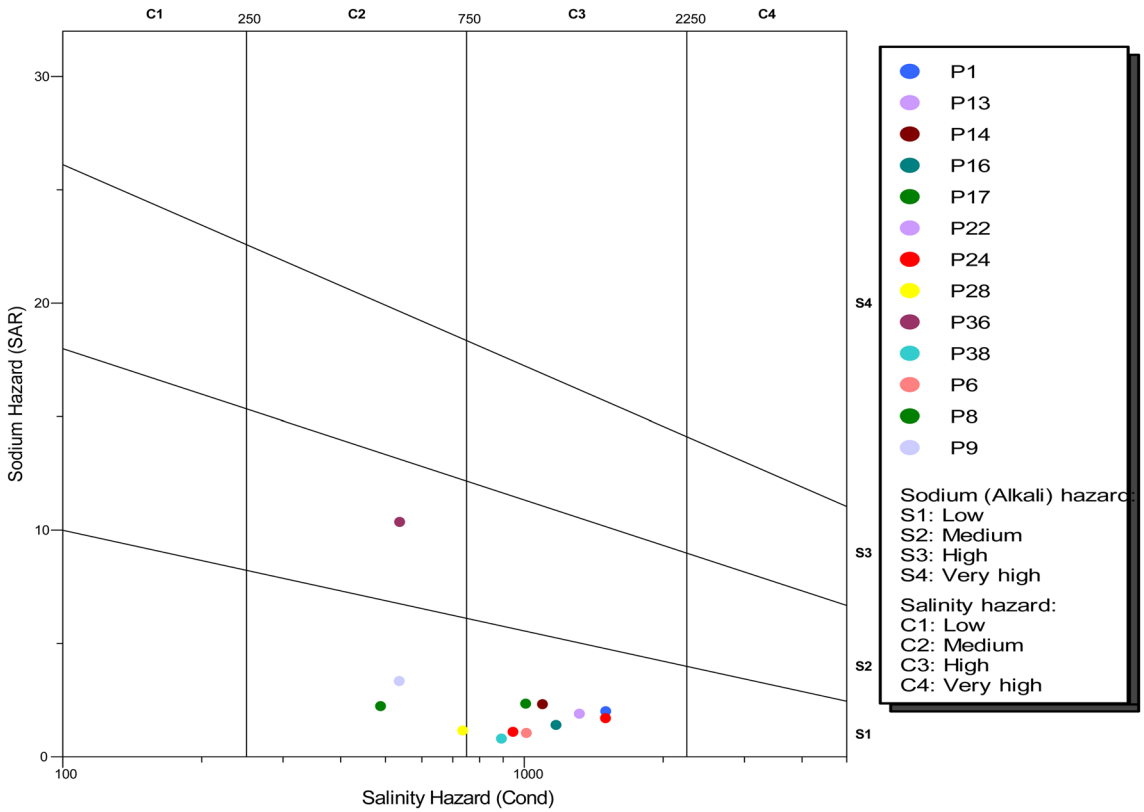

Fig. 11 Wilcox diagram for determining the suitability of water samples for irrigation

for the sustainability of economic activities as well as human and environmental health in the future, especially considering that mitigation is more expensive than prevention.

Compliance with ethical standards

Availability of data and material The data used to support the findings of this study are available from the corresponding author upon request.

References

Abou Zakhem B, Hafez R (2015) Heavy metal pollution index for groundwater quality assessment in Damascus Oasis. Syria. Environ Earth Sci 73(10):6591–6600. https://doi.org/10.1007/s12665-014-3882-5

Assubaie FN (2015) Assessment of the levels of some heavy metals in water in Alahsa Oasis farms, Saudi Arabia, with analysis by atomic absorption spectrophotometry. Arab J Chem 8(2):240–245. https://doi.org/10.1016/j.arabjc.2011.08.018

Atta R, Abida F, Tangfu X, Sajid M, Aqeel KM et al (2016) Elevated levels of arsenic and trace metals in drinking water of Tehsil Mailsi, Punjab, Pakistan. J Geochem Explor 169:89–99. https://doi.org/10.1016/j.gexplo.2016.07.013

Biswas A, Nath B, Bhattacharya P, Halder D, Kundu AK, Mandal U, Mukherjee A, Chatterjee D, Mörth CM, Jacks G (2012) Hydrogeochemical contrast between brown and grey sand aquifers in shallow depth of Bengal Basin: consequences for sustainable drinking water supply. Sci Total Environ 431:402–412. https://doi.org/10.1016/j.scitotenv.2012.05.031

Blanco Hernandez AL, Alonso GD, Jimenez de Blas O, Santiago G, M., De Miguel, M. B., (1998) Estudio de los niveles de plomo, cadmio, zinc y arsénico en aguas de la provincia de Salamanca. Rev Española de Salud Pública 72:53–65

Canora F, Rizzo G, Panariello S, Sdao F (2019) Hydrogeology and hydrogeochemistry of the Lauria mountains northern sector groundwater resources (Basilicata, Italy). Geofluids. https://doi.org/10.1155/2019/7039165 **(Article ID 7039165)**

Chowdhury S, Mazumder MAJ, Al-Attas O, Husain T (2016) Heavy metals in drinking water: Occurrences, implications, and future needs in developing countries. Sci Total Environ 569–570:476–488. https://doi.org/10.1016/j.scitotenv.2016.06.166

Corral-Bermúdez ML, Rivera-Quintero N, Sánchez- Ortiz E (2014) Percepciones y realidades de la contaminación en la comunidad minera San José de Avino. Durango Tecnol y Ciencias del Agua 5(5):125–140

De Zuane J (1993) Handbook of drinking water quality, 2nd edn. Wiley, New York, 575 p

Esteller MV, Kondratenko N, Expósito JL, Medina M, Martin del Campo-Delgado MA (2017) Hydrogeochemical characteristics of a volcanic-sedimentary aquifer with special emphasis on Fe and Mn content: a case study in Mexico. J Geochem Explor 180:113–126. https://doi.org/10.1016/j.gexplo.2017.06.002

EEC (2015) Standards of the quality of water intended for human consumption **(1998L0083-EN-27.10.2015-003.001-1)**

Fetter CW (2001) Applied hydrogeology. Prentice Hall, Englewood Cliffs

Freeze A, Cherry J (1979) Groundwater pollution. Prentice Hall, New Jersey

Galitskaya IV, Mohan KR, Krishna AK, Batrak GI, Eremina ON, Putilina VS, Yuganova TI (2017) Assessment of soil and groundwater contamination by heavy metals and metalloids in Russian and Indian megacities. Procedia Earth Planet Sci 17:674–677. https://doi.org/10.1016/j.proeps.2016.12.180

Galván-Mancilla SM (1996) Cartografía Hidrogeológica de la terraza baja entre Hualahuises y Linares, N.L. Universidad Autónoma de Nuevo León, Facultad de Ciencias de la Tierra, Tesis de Licenciatura, pp 115

Goldberg VM (1989) Groundwater pollution by nitrates from livestock wastes. Environ Health Perspect 83:25–29. https://doi.org/10.1289/ehp.898325

He B, He J, Wang L, Zhang X, Bi E (2019) Effect of hydrogeological conditions and surface loads on shallow groundwater nitrate pollution in the Shaying River Basin: Based on least squares surface fitting model. Water Res. https://doi.org/10.1016/j.watres.2019.114880

Horton RK (1965) An index number system for rating water quality. J Water Pollut Cont Fed 37(3):300–305

Huljek L, Perković D, Kovač Z (2019) Nitrate contamination risk of the Zagreb aquifer. J Maps 15(2):570–577. https://doi.org/10.1080/17445647.2019.1642248

Instituto Nacional de Estadística y Geografía (INEGI) (2015) Encuesta intercensal. www.inegi.gob.mx. Accessed 26 Feb 2020

Instituto Nacional de Estadística, Geografía e Informàtica (INEGI) (1999) Carta topografica G14C58 (Linares) escala 1:50 000 serie III. N.L

Jia X, O'Connor D, Hou D, Jin Y, Li G, Zheng C, Ok Y, Tsang D, Luo J (2019) Groundwater depletion and contamination: Spatial distribution of groundwater resources sustainability in China. Sci Total Environ. https://doi.org/10.1016/j.scitotenv.2019.03.457

Koh DCh, Chae GT, Kang BR, Koh GW, Park KH (2009) Baseline geochemical characteristics of groundwater in the mountains of Jeju Island, South Korea: implications for degree of mineralization and nitrate contamination. J Hydrol 376:81–93. https://doi.org/10.1016/j.j.hydrol.2009.07.016

Kwaya MY, Hamidu H, Mohammed AI, Abdulmumini YN, Adamu H, Grema HM et al (2019) Heavy metals pollution Indices and Multivariate Statistical Evaluation of Groundwater Quality of Maru town and environs. J Mater Environ Sci 10(1):32–44

Lang YC, Liu CQ, Zhao ZQ, Li SL, Han GL (2006) Geochemistry of surface and groundwater in Guiyang city, China: Water rock interaction and pollution in a karst hydrological system. Appl Geochem 21:887–903

Ling B (2000) Health impairments arising from drinking water polluted with domestic sewage and excreta in China. Schriftenreihe Des Vereins Für Wasser-, Boden-Und Lufthygiene 105:43–46

López Ramos E (1980) Geología de México tomo II: Provincia VI Noreste de México, Instituto de Geología de la UNAM, 2nd edn, pp 380

Marshall RE, Levison J, McBean EA, Parker B (2019) Wastewater impacts on groundwater at a fractured sedimentary bedrock site in Ontario, Canada: implications for First Nations' source-water protection. Hydrogeology J 27:2739–2753. https://doi.org/10.1007/s10040-019-02019-7

Mititelu-Ionuș O, Simulescu D, Popescu SM (2019) Environmental assessment of agricultural activities and groundwater nitrate pollution susceptibility: a regional case study (Southwestern Romania). Environ Monit Assess 191:501. https://doi.org/10.1007/s10661-019-7648-0

Nalawade PM, Bholay AD, Mule MB (2012) Assessment of groundwater and surface water quality indices for heavy metals nearby area of Parli Thermal Power Plant. Univ J Environ Res Technol 2(1):47–51

Navarro Galindo A (1959) Reconocimiento Geológico del área Montemorelos, Linares, General Terán, Estado de Nuevo León, Instituto Politécnico Nacional, Facultad de Ingeniería, Tesis de Ingeniería, pp 85

NOM-127-SSA1 (1994) Salud ambiental, agua para uso y consumo humano-límites permisibles de calidad y tratamientos a que debe someterse el agua para su pot- abilización. DOF (20 de junio de 2000)

Nordberg G, Langard S, Sunderman FW, Mager Stellman J, Osinsky D, Markkanen P (2001) Metales: propiedades quimicas y toxicidad. Enciclopedia de Salud y Seguridad En El Trabajo, pp 1–76

Ocampo-Astudillo A, Garrido-Hoyos SE, Salcedo-Sánchez ER, Martínez-Morales M (2020) Alteration of groundwater hydrochemistry due to its intensive xxtraction in urban areas from Mexico. In: Otazo-Sánchez E, Navarro-Frómeta A, Singh V (eds) Water availability and management in Mexico. Water Science and Technology Library, vol 88. Springer, Cham. https://doi.org/10.1007/978-3-030-24962-5_4

Otero V, Campos MF, Pinto JV, Vilarigues M, Carlyle L, Melo MJ (2017) Barium, zinc and strontium yellows in late 19th-early 20th century oil paintings. Heritage Sci 5(1):1–13. https://doi.org/10.1186/s40494-017-0160-3

Padilla-Sánchez RJ (1982) Geologic evolution of the Sierra Madre Oriental between Linares, Concepción del Oro, Saltillo and Monterrey, Mexico, University of Texas at Austin, Ph.D. Thesis

Pérez Castresana G, Castañeda Roldán E, García Suastegui WA, Morán Perales JL, Cruz Montalvo A, Handal Silva A (2019) Evaluation of health risks due to heavy metals in a rural population exposed to Atoyac River pollution in Puebla, Mexico. Water 11(2):277

Pujari PR, Padmakar C, Labhasetwar PK, Mahore P, Ganguly AK (2012) (2012) Assessment of the impact of on-site sanitation systems on groundwater pollution in two diverse geological settings—a case study from India. Environ Monit Assess 184:251–263. https://doi.org/10.1007/s10661-011-1965-2

Purushotham D, Linga D, Sagar N, Mishra S, Naga Vinod G, Venkatesham K, Saikrishna K (2017) Groundwater contamination in parts of Nalgonda district, Telangana, India as revealed by trace elemental studies. J Geol Soc India 90(4):447–458. https://doi.org/10.1007/s12594-017-0738-0

Ramakrishnaiah CR, Sadashivaiah C, Ranganna G (2009) Assessment of water quality index for the groundwater in Tumkur taluk, Karnataka state. India E J Chem 6(2):523–530. https://doi.org/10.1155/2009/757424

Rajmohan N, Patel N, Singh G, Amarasinghe UA (2017) (2017) Hydrochemical evaluation and identification of geochemical processes in the shallow and deep wells in the Ramganga Sub-Basin, India. Environ Sci Pollut Res 24:21459–21475. https://doi.org/10.1007/s11356-017-9704-z

Rangel-Rodríguez MM (1989) Hidrogeología de la Ciudad Universitaria de la Universidad Autónoma de Nuevo León, Linares, México, Technische Hochschule Darmstadt, Diplomarbeit, pp 108

Ravindra K, Thind PS, Mor S, Singh T, Mor S (2019) Evaluation of groundwater contamination in Chandigarh: Source identification and health risk assessment. Environ Pollut. https://doi.org/10.1016/j.envpol.2019.113062

Rivera-Rodríguez DA, Beltrán-Hernández RI, Lucho-Constantino CA et al (2019) Water quality indices for groundwater impacted by geogenic background and anthropogenic pollution: case study in Hidalgo. Mex Int J Environ Sci Technol 16:2201–2214. https://doi.org/10.1007/s13762-018-1852-2

Rasool A, Xiao T, Farooqi A, Shafeeque M, Masood S, Ali S,Fahad S, Nasim W (2016) Arsenic and heavy metal contaminations in the tube well water of Punjab, Pakistan and risk assessment: A case study. Ecol Eng 95:90–100

Salcedo Sánchez ER, Garrido Hoyos SE, Esteller MV, Martínez Morales M, Ocampo Astudillo A (2017) Hydrogeochemistry and water-rock interactions in the urban area of Puebla Valley aquifer (Mexico). J Geochem Explor 181:219–235. https://doi.org/10.1016/j.gexplo.2017.07.016

Sheykhi V, Moore F (2012) Geochemical characterization of Kor River Water Quality, Fars Province, Southwest Iran. Water Qual Exposure Health 4(1):25–38. https://doi.org/10.1007/s12403-012-0063-1

Smoroń S (2016) Quality of shallow groundwater and manure effluents in a livestock farm. J Water Land Dev 29(1):59–66. https://doi.org/10.1515/jwld-2016-0012

Tiwari AK, Singh PK, Singh AK, De Maio M (2016) Estimation of heavy metal contamination in groundwater and development of a heavy metal pollution index by using GIS technique. Bull Environ Contam Toxicol 96(4):508–515. https://doi.org/10.1007/s00128-016-1750-6

U.S. EPA (2018) Edition of the drinking water standards and health advisories tables. EPA 822-F-18-001

Venkata Mohan S, Nithila P, Jayarama Reddy S (1996) Estimation of heavy metals in drinking water and development of heavy metal pollution index. J Environ Sci Health Part A Toxic Hazard Subst Environ Eng 31(2):283–289. https://doi.org/10.1080/10934529609376357

WHO (2017) Guidelines for drinking-water quality: fourth edition incorporating the first addendum. Geneva: World Health Organization. Licence: CC BY-NC-SA 3.0 IGO **(ISBN 978-92-4-154995-0)**

Wilburn DR (2008) Material Use in the United States-Selected Case Studies for Cadmium, Cobalt, Lithium, and Nickel in Rechargeable Batteries. US Geol Surv Sci Investig Rep 5141:1–43. https://doi.org/10.1016/j.soncn.2015.08.007

Ximenes M, Duffy B, Faria MJ, Neely K (2018) Initial observations of water quality indicators in the unconfined shallow aquifer in Dili City, Timor-Leste: suggestions for its management. Environ Earth Sci 77(19)

Zhai Y, Zhao X, Teng Y, Li X, Zhang J, Wu J, Zuo R (2017) Groundwater nitrate pollution and human health risk assessment by using HHRA model in an agricultural area, NE China. Ecotoxicol Environ Saf. https://doi.org/10.1016/j.ecoenv.2016.11.010